Magneto-optical effect near the *D*1 resonance of spin-polarized cold cesium atoms

Jai Min Choi, Jang Myun Kim, Je Hyun Lee, Q-Han Park, and D. Cho*
Department of Physics, Korea University, Seoul 136-701, Korea
(Received 23 November 2004; published 22 April 2005)

We report our study of the magneto-optical effect in a strictly linear regime on spin-polarized cold cesium atoms. Due to the low intensity and the short illumination period of the probe beam, less than 7.5% of the sample atoms change their states by absorbing probe photons. We produce a medium of atoms at rest in either the $6S_{1/2}, F=3, m_F=0$ or $6S_{1/2}, F=3, m_F=3$ state by optically pumping atoms trapped in a magneto-optical trap. We use the *D*1 resonance with large lower and upper state hyperfine splittings as a probe transition to avoid hyperfine mixing from the Zeeman interaction. Under this idealized situation we measure the Stokes parameters in order to find the polarization rotation and circular dichroism experienced by the probe light. We find that there are qualitative differences between the results for the $m_F=0$ and $m_F=3$ cases. While dispersion and consequent Faraday rotation play a dominant role when the atoms are in the $m_F=0$ state, it is dissipation and circular dichroism that are important when they are in the $m_F=3$ state. Similarly, while the size of the Faraday rotation and the circular dichroism for the $m_F=0$ case scales linearly with the applied magnetic field, for the $m_F=3$ case it is the shift of the probe polarization change versus frequency that is linearly proportional to the magnetic field strength.

DOI: 10.1103/PhysRevA.71.043409 PACS number(s): 33.55.Ad, 42.50.Gy, 42.25.Ja

I. INTRODUCTION

The magneto-optical effect is a rotation of polarization when linearly polarized light passes through either a magnetized medium or a medium in a dc magnetic field. When the magnetization of the medium produces the rotation, it is called paramagnetic rotation, and when the applied magnetic field is responsible for the rotation, it is called the Faraday effect [1]. An optical isolator using a paramagnetic crystal placed in a permanent magnet is a well known application of the Faraday effect. When the medium is an atomic vapor, due to the low atom density it is necessary to use near resonant light in order to observe the Faraday rotation. The enhanced Faraday effect near resonance is known as the Macaluso-Corbino effect [2]. Both the Faraday effect and the Macaluso-Corbino effect have been known for more than 100 years. However, there is still much interest in these effects because they can be used for the sensitive study of collision dynamics [3] and for precision measurement in search of fundamental symmetry violations [4]. Current research involving the resonant magneto-optic effect using a gaseous atomic medium is reviewed in Ref. [5].

While the resonant interaction between an atom and a probe light makes the magneto-optical effect observable, it also leads to significant absorption of the probe light by the atoms. There are two major complications coming from the large absorption. First, the atomic medium is optically pumped by the linear probe light and consequently the property of the medium is determined by the probe light itself. This nonlinear situation, coupled with an applied magnetic field, leads to complex manifestation of the Hanle effect [6] and various Zeeman coherences [7]. Second, a large circular dichroism is unavoidable. Faraday rotation in its original form relies on a difference in the indices of refraction for the right (σ^+) and the left circularly polarized (σ^-) components of linear light, i.e., the differential dispersion from the difference in the real parts of electric susceptibilities of the medium. When the probe frequency is near resonance, however, the imaginary parts of the susceptibilities are large and in general asymmetric with respect to the $\sigma+$ and $\sigma-$ components, leading to a differential dissipation of the two components. Consequently, the output polarization of the probe light is a result of a complicated interplay between the magneto-optic rotation and the circular dichroism.

There have been studies on the resonant Faraday effect using an atomic vapor cell [8] or cold atoms prepared by a magneto-optical trap (MOT) [9]. Although relatively low-intensity probe light was used in the referred work, for the experimental parameters employed in the experiments each atom in the probe region absorbed on average more than one photon while the probe beam was on. An arbitrary distribution of atoms among Zeeman sublevels also meant that different contributions to magneto-optic rotation and circular dichroism from atoms in various sublevels are mixed up in the final result. These factors, together with Doppler broadening for the case of the cell experiment, mixing of the upper hyperfine states from Zeeman coupling, and depolarization from the laser linewidth [10], produced a rather complicated experimental situation and made quantitative understanding of the results difficult.

In order to avoid these difficulties we study the resonant magneto-optical effect in a strictly linear regime on spin-polarized cold cesium atoms prepared by optically pumping trapped atoms. By optically pumping the atoms to either $m_F=0$ or $m_F=3$ sublevels, where m_F is the magnetic quantum number, we can clearly distinguish contributions to the magneto-optic rotation and the circular dichroism from atoms in each spin-polarized state. We also use the cesium *D*1 transition, whose upper state, $6P_{1/2}$, has large hyperfine split-

*Email address: cho@korea.ac.kr

ting, in order to avoid complication from hyperfine mixing. Our laser linewidth is also only 1/20 of the natural linewidth of the $D1$ transition and depolarization from the laser linewidth is thus minimized.

II. THEORY

Considering cesium transitions from the $|6S_{1/2},F=3,m_F\rangle$ state to the $|6P_{1/2},F=4,m_F\pm1\rangle$ states, where F is the total angular momentum, driven by the $\sigma+$ and $\sigma-$ components of linearly polarized light when a magnetic field B is applied along the z axis, the complex indices of refraction for the $\sigma\pm$ light are

$$n_\pm \cong 1+\frac{N}{2\hbar\epsilon_0}\frac{|\langle 6P_{1/2},F=4,m_F\pm1|D_\pm|6S_{1/2},F=3,m_F\rangle|^2}{\omega_\pm(B)-\omega-i\Gamma/2}, \tag{1}$$

where N is the atom number density; $D_\pm$ are the electric dipole moment operators; Γ is the decay rate of the $6P_{1/2}$ state; ω is the laser frequency; and $\omega_\pm(B)$ is the Zeeman-shifted resonance frequency, $\omega_{D1}+(\mu_B B/\hbar)\{g_F'(m_F\pm1)-g_F m_F\}$ for $\sigma\pm$ components. Here ω_{D1} is the unperturbed $D1$ resonance frequency, μ_B is the Bohr magneton, and g_F and g_F' are the Lande g factors of the lower and the upper states, respectively. When atoms in a medium are distributed among different m_F sublevels with fractional populations $p(m_F)$, the second term of the above expression should be a sum of the corresponding terms weighted by $p(m_F)$.

When the probe beam propagating along the z axis is initially linearly polarized along the x axis with its field amplitude $E_0\hat{x}$, its output polarization from the atomic medium can be written as

$$\vec{E}_{\text{out}}=\frac{E_0}{\sqrt{2}}(\hat{\epsilon}_+e^{i\beta_+-1/2\alpha_+}+\hat{\epsilon}_-e^{i\beta_--1/2\alpha_-}), \tag{2}$$

where $\hat{\epsilon}_\pm$ are the unit vectors for the $\sigma\pm$ polarizations, and the absorption coefficients $\alpha_\pm$ and phase shifts $\beta_\pm$ are defined by

$$\alpha_\pm = 2kl\ \text{Im}(n_\pm),$$

$$\beta_\pm = kl\ \text{Re}(n_\pm).$$

Here k is the wave vector in vacuum and l is the length of the atomic medium along the probe propagation. When the output polarization is depicted by Fig. 1, the rotation angle ψ is related to $\beta_\pm$ by

$$\psi=\tfrac{1}{2}(\beta_+-\beta_-). \tag{3}$$

The ellipticity of the ellipse in Fig. 1 can be characterized by an auxiliary angle χ with $\tan\chi=b/a$ [11]. χ is related to $\alpha_\pm$ by

$$\sin 2\chi=\frac{e^{-\alpha_+}-e^{-\alpha_-}}{e^{-\alpha_+}+e^{-\alpha_-}}. \tag{4}$$

The above expression for $\sin 2\chi$ can be considered as a definition for a degree of circular dichroism of the medium. We also note that the rotation angle is determined by the dispersive property of the medium, while the ellipticity is determined by the dissipative property. In Fig. 2. the relative transition strengths from the $|6S_{1/2},F=3,m_F\rangle$ states to the $|6P_{1/2},F=4,m_F\pm1\rangle$ states are given. We note that when $m_F\neq0$, there are large differences between the $\sigma+$ and the $\sigma-$ transition strengths. This implies that when an atomic medium is oriented, circular dichroism is the dominant process. Only a medium without orientation can produce pure Faraday rotation, and a sample of atoms spin polarized with $m_F=0$ is an example.

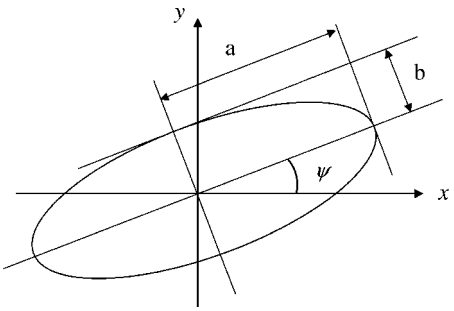

FIG. 1. Output polarization. ψ is the rotation angle determined by $\beta_\pm$. Ellipticity is characterized by the auxiliary angle χ with $\tan\chi=b/a$. A degree of circular dichroism $\sin 2\chi$ is determined by $\alpha_\pm$.

In the experiment we measure the parallel, perpendicular, +45°, −45°, $\sigma+$, and $\sigma-$ components of the output beam, which we denote by $P_\parallel$, $P_\perp$, P_{+45}, P_{-45}, $P_{\sigma+}$, and $P_{\sigma-}$, respectively. Both $\tan 2\psi$ and $\sin 2\chi$ are related to these components by the following relations:

$$\tan 2\psi=\frac{P_{+45}-P_{-45}}{P_\parallel-P_\perp} \tag{5}$$

$$\sin 2\chi=\frac{P_{\sigma+}-P_{\sigma-}}{P_{\sigma+}+P_{\sigma-}}. \tag{6}$$

These relations are usually given in terms of Stokes parameters [11].

III. APPARATUS

A cold cesium sample is produced by a conventional vapor cell MOT, which is built around an octagonal ultrahigh vacuum chamber. Heated dispensers provide cesium vapor

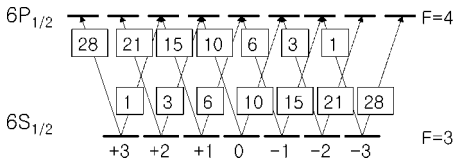

FIG. 2. Relative transition strengths from the $|6S_{1/2},F=3,m_F\rangle$ states to the $|6P_{1/2},F=4,m_F\pm1\rangle$ states. The numbers in the boxes are $24|\langle 6P_{1/2},F=4,m_F\pm1|D_\pm|6S_{1/2},F=3,m_F\rangle|^2/|\langle 6P_{1/2},F=4\|D\|6S_{1/2},F=3\rangle|^2$, where $\langle 6P_{1/2},F=4\|D\|6S_{1/2},F=3\rangle$ is the reduced matrix element.

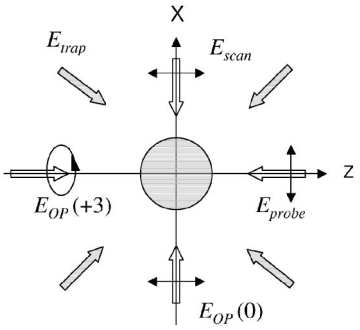

FIG. 3. Orientation of the quantization field and optical fields. Trapping beams for the MOT, which are also used for the hyperfine pumping, are shown with shaded arrows. $E_{OP}(0)$ and $E_{OP}(+3)$ are the Zeeman pumping beams for the target states of $m_F=0$ and $m_F=3$, respectively. E_{scan} is used to monitor the results of the optical pumping and E_{probe} is the probe field for the Faraday rotation.

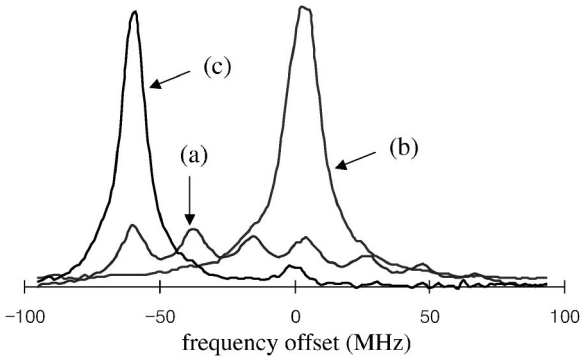

FIG. 4. Distribution of atoms among the $|6S_{1/2},F=3,m_F\rangle$ sublevles: (a) the sample with only the hyperfine pumping, (b) the sample pumped into the $m_F=0$ sublevel, and (c) the sample pumped into the $m_F=3$ sublevel.

and two external-cavity diode lasers provide trapping and repumping beams. The vapor cell MOT system is described in our previous publication [12]. In addition to the anti-Helmholtz coil for the MOT, we have three sets of Helmholtz coils to counteract the ambient magnetic field. The quantization field B for the optical pumping and the Faraday rotation is provided by a single coil of 400 turns and 30 cm diameter, placed 4.5 cm from the MOT center. B defines the z axis in Fig. 3, where the optical layout of the experiment is shown.

For the optical pumping we use two laser beams. One of them is tuned to the $6S_{1/2},F=4\rightarrow 6P_{3/2},F=4$ transition and it pumps the atoms in the $6S_{1/2},F=4$ state to the $6S_{1/2},F=3$ state. It is called hyperfine pumping. We use the trapping beam, E_{trap} in Fig. 3, as the hyperfine pumping beam by shifting its frequency during the optical pumping. Another one is tuned to the $6S_{1/2},F=3\rightarrow 6P_{1/2},F=3$ transition and it is called the Zeeman pumping beam. As the Zeeman pumping beam, we use $E_{OP}(0)$ with linear polarization or $E_{OP}(+3)$ with circular polarization in Fig. 3 when the target state is $|6S_{1/2},F=3,m_F=0\rangle$ or $|6S_{1/2},F=3,m_F=3\rangle$, respectively. Its intensity is 0.5 mW/cm^2 and its diameter is 5 mm. In order to measure the Zeeman distribution of atoms after the optical pumping, we take a part of the repumping beam and scan it near the $6S_{1/2},F=3\rightarrow 6P_{3/2},F=4$ transition. It is shown as E_{scan} in Fig. 3. Finally we use another diode laser tuned to the $6S_{1/2},F=3\rightarrow 6P_{1/2},F=4$ transition as a probe laser, E_{probe}, to study the Faraday effect. The probe laser beam is spatially filtered and transferred to the chamber by an optical fiber. Its power is turned on and off by an acousto-optic modulator.

In order to jump or scan the trapping, repumping, and probe laser frequencies we use individual dichroic-atomic-vapor-laser-locking (DAVLL) systems [13] for each laser. A DAVLL system provides a stable reference signal over the relevant frequency range. We employ an injection-current feed forward system, which allows us to relock the laser to a new frequency within a fraction of a millisecond. We also have a conventional saturated absorption spectrometer for each laser to monitor its exact frequency.

IV. OPTICAL PUMPING

Each measurement cycle begins with 3×10^8 cesium atoms at 200 μK collected by a MOT. At the end of the MOT loading period of 0.7 s the frequencies of the trapping and the repumping lasers are moved away from the respective resonances by more than 100 MHz and the repumping beam shutter is closed within 1 ms. It is followed by switching off of the anti-Helmholtz coil. For the next 3 ms the quantization field is turned on to 13 G, and the magnetic field from the anti-Helmholtz coil tails off. Then the frequency of the trapping laser is brought to the hyperfine pumping transition. Simultaneously, the Zeeman pumping laser, with proper polarization, is turned on. Both hyperfine and Zeeman pumping beams are on for 2 ms and this completes the optical pumping process.

Results of the optical pumping are shown in Fig. 4. To obtain the Zeeman spectra we increase the quantization field to 30 G and illuminate the sample with E_{scan} while scanning it over 200 MHz near the $6S_{1/2},F=3\rightarrow 6P_{3/2},F=4$ transition. We use this transition because of the large difference between the Lande g factors of the two states. The Lande g factor of the $6S_{1/2},F=3$ state is $-1/4$ while that of the $6P_{3/2},F=4$ state is $4/15$. The laser field E_{scan} is linearly polarized along the z axis so that it can drive $\Delta m_F=0$ transitions only. Adjacent Zeeman components of the transition are shifted from each other by 22 MHz at 30 G, which is much larger than the natural linewidth of the $D2$ transition, so the probe laser can drive only one Zeeman component at a time. Once the atoms are driven to the $6P_{3/2},F=4$ state, they decay to the $6S_{1/2},F=4$ state with the branching ratio of $7/12$. Finally, the quantization field is turned off and the trapping laser, tuned to the cycling transition, is turned on. We integrate the fluorescence from the cycling transition for 1 ms to measure the number of atoms in the upper hyperfine state. This measurement is destructive and the optical pumping cycle has to be repeated for each data point of the spectrum.

In this measurement, atoms driven to the $6P_{3/2},F=4$ state can decay back down to the $6S_{1/2},F=3$ state with $5/12$ probability. If the atom falls back to the original Zeeman sublevel, it can make another round of the $D2$ transition, and it still has a chance to contribute to the final fluorescence. If it

falls back to adjacent Zeeman sublevels, however, it is lost. Considering the branching ratios to different Zeeman sublevels, we can calculate the detection efficiency for each Zeeman sublevel of the $6S_{1/2},F=3$ state. They range from a minimum of 65% for $m_F=\pm 3$ to a maximum of 77% for $m_F=0$.

Curve (a) in Fig. 4 shows the Zeeman spectrum with the hyperfine pumping only. The seven peaks from the Zeeman sublevels are clearly resolved. We note that the Zeeman distribution is skewed toward $m_F=3$. It is reproducible in our MOT and it is due to the residual intensity imbalance and polarization asymmetry of the trapping beams. Curves (b) and (c) show the results of the optical pumping into the $|6S_{1/2},F=3,m_F=0\rangle$ state and the $|6S_{1/2},F=3,m_F=3\rangle$ state, respectively. In both cases more than 90% of the atoms are pumped to the desired state.

V. RESONANT MAGNETO-OPTICAL EFFECT

Before we study the resonant Faraday effect on the spin-polarized atomic sample, we conduct preliminary measurements to make sure that our experimental situation is in the linear regime. The probe power is 6.4 nW and it is illuminated for 400 μs. When the sample is spin polarized to $m_F=0$, approximately 90% of the power is absorbed at resonance, which corresponds to the absorption of 1.0×10^7 photons. The measured optical thickness of the sample is 9 [14]. From the probe beam diameter of 2 mm, this corresponds to 6.6×10^7 atoms. As a result, the fraction f of atoms in the probe region that absorb at least one photon is 15%. As an independent check, we measure the number of atoms pumped to the $6S_{1/2},F=4$ state by the probe light. We find 5% of the sample atoms in the $6S_{1/2},F=4$ state after the probe illumination. Considering the branching ratios of the decay from the $6P_{1/2},F=4$ state, it implies that the fraction f is 12%. Taking into account the fact that a significant part of the absorption and consequent decay bring the atoms back to the original state and considering the time average over the probe illumination period, the effective fraction of atoms perturbed by the probe light is only 5%. For the experiment with atoms optically pumped to the $|6S_{1/2},F=3,m_F=3\rangle$ state, we use the sample with similar atom density and cloud size so that Nl remains the same. Because the sum of the $\Delta m_F=\pm 1$ transition strengths out of the $m_F=3$ state is roughly 50% larger than that of the $m_F=0$ state (Fig. 2), the optical thickness in this case is close to 13, and the effective perturbed fraction is 7.5%.

Results of the polarization measurements with the $m_F=0$ sample when the B field is 20 G are shown in Fig. 5. Figure 5 gives (a) $P_{\|}$, $P_{\perp}$; (b) P_{+45}, P_{-45}; and (c) $P_{\sigma+}$, $P_{\sigma-}$, normalized to the transmitted power when there are no atoms. Figure 5(d) shows the rotation angle ψ, Eq. (3), in radians and the degree of circular dichroism $\sin 2\chi$, Eq. (4). Theoretical curves are shown with solid and dotted lines. There are no fitting parameters for the theory curves other than the optical thickness and the fractional populations $p(m_F)$, which are measured independently. We use the optical thickness of 9 and the fractional populations, $p(0)=0.9$ and $p(\pm 1)=0.05$. Similar results are shown in Fig. 6 for the $m_F=3$ sample

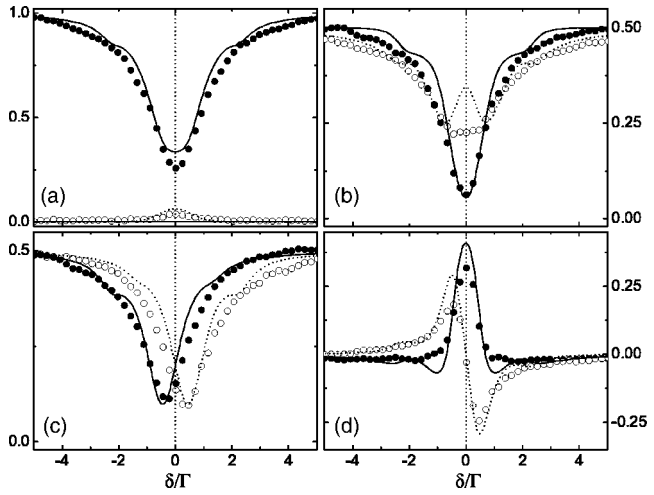

FIG. 5. Results of the polarization measurements with the $m_F=0$ sample. (a) $P_{\|}$(●) $P_{\perp}$(○), (b) P_{+45}(●), P_{-45}(○), and (c) $P_{\sigma+}$(●), $P_{\sigma-}$(○). Each component is normalized to the total transmitted power when there are no atoms. (d) the rotation angle ψ in radians (●) and the degree of circular dichroism $\sin 2\chi$ (○). Theoretical curves are shown with solid and dotted lines.

under the same magnetic field. The fractional populations are $p(3)=0.9$, $p(2)=0.07$, and $p(1)=0.03$. Data sets shown in Figs. 5 and 6 are redundant in that they contain three pairs of orthogonal polarization channels. Sums of each pair are compared. They agree with each other except for the quarter waveplate insertion loss for the $P_{\sigma+}$, $P_{\sigma-}$ channels. In most of the data the measured results reproduce theoretical results reasonably well. Residual discrepancies are attributable to: (i) magnetic field inhomogeneity, (ii) transient frequency jittering of the probe laser, and (iii) fluctuations of the number of optically pumped MOT atoms.

By comparing Fig. 5(d) for $m_F=0$ and Fig. 6(d) for $m_F=3$, we note that there is a drastic difference between the two cases. In addition to the obvious shift of the curves due to the Zeeman shift, the parities of ψ and $\sin 2\chi$ are even and odd, respectively, for $m_F=0$, while they are odd and even for

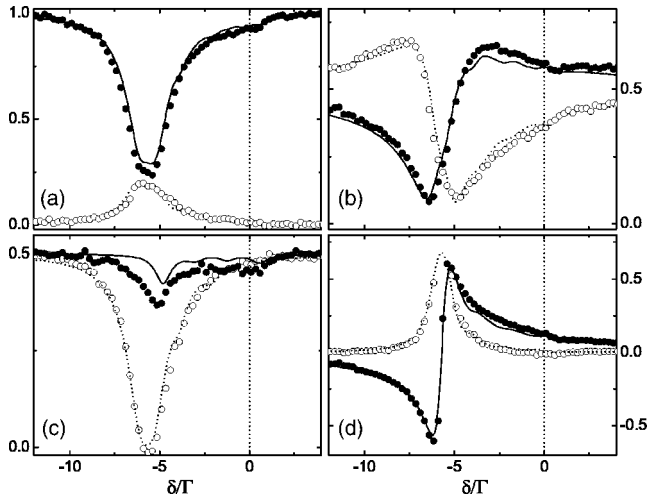

FIG. 6. Results of the polarization measurements with the $m_F=3$ sample.

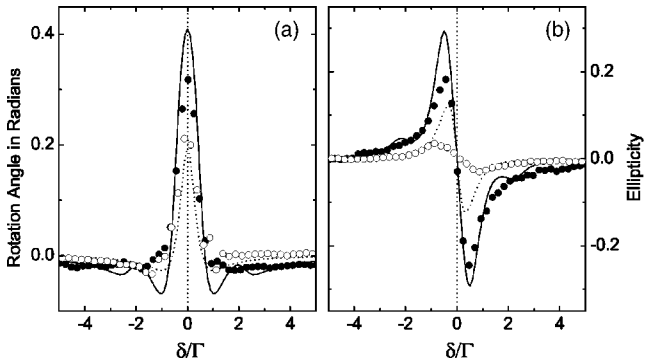

FIG. 7. Measurement results and theoretical curves for the the case of $m_F=0$ state with high and low magnetic fields: (a) the rotation angle ψ in radians and (b) the degree of circular dichroism $\sin 2\chi$ for $B=20$ G (●) and $B=5$ G (○).

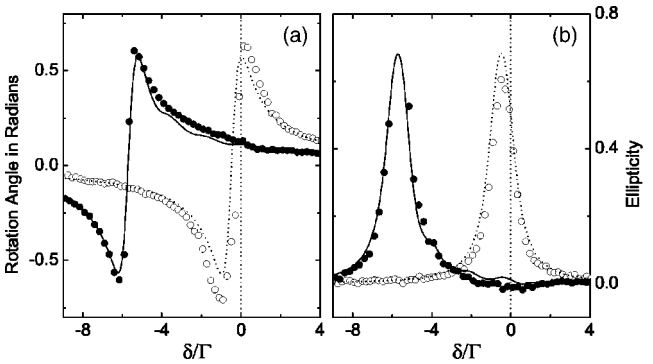

FIG. 8. Measurement results and theoretical curves for the case of $m_F=3$ state with $B=20$ G (●) and $B=2$ G (○).

$m_F=3$ with respect to its resonance. For the atoms in the $m_F=0$ state under a magnetic field, the phase angles $\beta_\pm$ for $\sigma\pm$ couplings are of similar size and opposite signs near resonance and they add up in determining ψ. Because the $\sigma+$ and $\sigma-$ coupling strengths are the same (Fig. 2), the absorption coefficients are also of similar size and the circular dichroism is small near resonance. On the other hand, the ratio of the $\sigma+$ and $\sigma-$ coupling strengths for $m_F=3$ atoms are 28:1. Near a Zeeman-shifted resonance the $\sigma+$ component is almost completely absorbed, while the $\sigma-$ component is not attenuated much. This leads to a large circular dichroism and the output polarization is near left circular polarization. Although dispersion and dissipation are closely connected by the Kramers-Kronig relations, we may conclude that dispersion plays a dominant role in the $m_F=0$ case, while it is the dissipation that is important for the $m_F=3$ case. In the resonant Faraday effect experiments performed with unpolarized atomic samples [8,9], the contributions from atoms in different Zeeman sublevels are averaged and resulting spectra for ψ and $\sin 2\chi$ are a somewhat broadened version of Fig. 5(d). The average spectra do not give much information on relative contributions from dispersion and dissipation coming from various Zeeman sublevels.

Another major difference between the $m_F=0$ and $m_F=3$ cases is that while for the former case it is the magnetic field that gives rise to the Faraday rotation, for the latter case the magnetization of the medium itself produces paramagnetic rotation of the probe polarization. In order to demonstrate this point we repeat the measurements at a lower magnetic field. The results for the $m_F=0$ state with $B=20$ and 5 G are shown in Fig. 7. Similar results for the $m_F=3$ case with $B=20$ and 2 G are shown in Fig. 8. Comparing the results with the high and low magnetic fields in Fig. 7, we note that when atoms are in the $m_F=0$ state, the size of both the Faraday rotation and the circular dichroism is linearly proportional to the applied magnetic field strength. On the other hand, we find from Fig. 8 that when atoms are in the $m_F=3$ state, the size of the polarization rotation and circular dichroism is largely independent of the field strength as expected for the paramagnetic rotation. Instead, it is the shift of the probe polarization change versus frequency that is linearly proportional to B for this case. From our measurement we find that, in a strict sense, the Verdet constant has a meaning only when the atomic medium is without orientation.

VI. CONCLUSION

We study the resonant magneto-optic effect under an idealized situation. We use a probe light with a very low intensity and short duration to avoid the nonlinear effect and spin-polarized cold atoms to avoid complications from Zeeman distribution and Doppler broadening. By comparing output polarizations from the medium of atoms in the $m_F=0$ and 3 states we find that there are qualitative differences in dispersive and dissipative properties of the medium, depending on their spin-polarization state and consequent magnetization.

ACKNOWLEDGMENT

This work was supported by the Ministry of Education (Grant No. 2001-015-DP0107). J.M.C. acknowledges support from the Korea Optical Industry Inc.

[1] M. Faraday, *Experimental Research* (London, 1855), Vol. III, p. 2164.
[2] M. Macaluso and O. M. Corbino, Nuovo Cimento **8**, 257 (1898).
[3] J. P. Woerdman, F. J. Blok, M. Kristensen, and C. A. Schrama, Phys. Rev. A **53**, 1183 (1996).
[4] D. Budker, V. Yashchuk, and M. Zolotorev, Phys. Rev. Lett. **81**, 5788 (1998).
[5] D. Budker, W. Gawlik, D. F. Kimball, S. M. Rochester, V. V. Yashchuk, and A. Weis, Rev. Mod. Phys. **74**, 1153 (2002).
[6] S. I. Kanorsky, A. Weis, J. Wurster, and T. W. Hänsch, Phys. Rev. A **47**, 1220 (1993).
[7] D. Budker, D. F. Kimball, S. M. Rochester, and V. V. Yashchuk, Phys. Rev. Lett. **83**, 1767 (1999).

[8] X. Chen, V. L. Telegdi, and A. Weis, J. Phys. B **20**, 5653 (1987).
[9] G. Labeyrie, C. Miniatura, and R. Kaiser, Phys. Rev. A **64**, 033402 (2001); S. Franke-Arnold, M. Arndt, and A. Zeilinger, J. Phys. B **34**, 2527 (2001).
[10] G. S. Agarwal and S. Dasgupta, Phys. Rev. A **67**, 063802 (2003).
[11] M. Born and E. Wolf, *Principles of Optics*, 6th ed. (Pergamon, New York, 1980).
[12] J. Y. Kim and D. Cho, J. Korean Phys. Soc. **39**, 864 (2001).
[13] K. L. Corwin, Z. T. Lu, C. F. Hand, R. J. Epstain, and C. E. Wieman, Appl. Opt. **37**, 3295 (1998).
[14] When absorption is more than 90%, absorbed fraction of power is not a reliable measure of the optical thickness. We inferred the optical thickness from the spectral width of the absorption spectrum.